Estuarine, Coastal and Shelf Science 184 (2017) 126–137

Estuarine circulation-driven entrainment of oceanic nutrients fuels coastal phytoplankton in an open coastal system in Japan

Kenta Watanabe[a,*], Akihide Kasai[b], Koji Fukuzaki[c], Masahiro Ueno[d], Yoh Yamashita[d,e]

[a] Coastal and Estuarine Environment Research Group, Port and Airport Research Institute, 3-1-1 Nagase, Yokosuka, Kanagawa 239-0826, Japan

[b] Division of Marine Bioresource and Environmental Science, Graduate School of Fisheries Sciences, Hokkaido University, 3-1-1 Minato-cho, Hakodate, Hokkaido 041-8611, Japan

[c] Division of Forest and Biomaterials, Graduate School of Agriculture, Kyoto University, Oiwake, Sakyo, Kyoto 606-8502, Japan

[d] Field Science Education and Research Center, Kyoto University, Nagahama, Maizuru, Kyoto 625-0086, Japan

[e] Field Science Education and Research Center, Kyoto University, Oiwake, Kitashirakawa, Sakyo, Kyoto 606-8502, Japan

* Kenta Watanabe (corresponding author)

e-mail: watanabe-ke@ipc.pari.go.jp, tel: +81-46-844-5046, fax: +81-46-844-1274

Abstract

We investigated interactions among seasonal fluctuations in phytoplankton biomass, riverine nutrient flux, and the fluxes of nutrients entrained by estuarine circulation in Tango Bay, Japan, to determine the influence of freshwater inflows to an open bay on coastal phytoplankton productivity. The riverine nutrient flux was strongly regulated by river discharge. Estuarine circulation was driven by river discharge, with high fluxes of nutrients (mean nitrate+nitrite flux: 5.3±3.5 Mg [mega grams]-N day^{-1}) between winter and early spring, enhanced by nutrient supply to the surface water via vertical mixing. In contrast, low-nutrient seawater was delivered to the bay between late spring and summer (1.0±0.8 Mg-N day^{-1}). Seasonal fluctuations in phytoplankton biomass were affected by the entrained fluxes of oceanic nutrients and variation in the euphotic zone depth, and to a lesser degree by the riverine nutrient flux. Bioassays and stoichiometric analyses indicated that phytoplankton growth was limited by nitrogen and/or phosphorus. Both the entrainment of oceanic nutrients and the euphotic zone depth affected the duration and magnitude of blooms. Our findings show that, unlike semi-enclosed bays, seasonal variations in coastal phytoplankton in an open coastal system are primarily fueled by the entrainment of oceanic nutrients and are influenced by both freshwater inflow and coastal conditions (e.g. vertical mixing and wind events).

Keywords

phytoplankton blooms; open bay; river discharge; nutrients; estuarine circulation; Japan, Kyoto, Tango Bay

1. Introduction

The global distributions of fishery resources correspond to the distributions of phytoplankton biomass, indicating that phytoplankton production supports fishery production in marine ecosystems (Caddy and Bakun, 1994) through a bottom-up effect (Kimmerer, 2002; Connolly et al., 2009; Kostecki et al., 2010). Because phytoplankton primary production is primarily limited by nutrient and light availability, variations in these factors regulate seasonal and annual fluctuations in phytoplankton primary production (Cloern and Jassby, 2008). The timing of phytoplankton blooms then regulates the timing of increases in secondary production, which affects larval fish survival and annual fish stock recruitment (Cloern and Jassby, 2008).

In estuarine and coastal systems without strong tidal mixing, freshwater flow and upwelling are the major processes supplying nutrients (Caddy and Bakun, 1994). In addition to directly transporting terrestrial nutrients, freshwater inflows also drive estuarine circulation, indirectly regulating the entrainment of oceanic nutrients from the offshore to coastal zones (Smith and Demaster, 1996). Seasonal and interannual variations in freshwater flow can strongly influence variability in coastal phytoplankton production (Cloern, 1996). Previous studies in semi-enclosed coastal systems have suggested that riverine nutrient inputs directly stimulate primary production (Paerl et al., 1990; Scharler and Baird, 2005), and that nutrient loadings that accompany seasonal floods drive phytoplankton blooms (Malone et al., 1988; Mallin et al., 1993; Sugimoto et al., 2004; Murrell et al., 2007). Moreover, the entrainment of recycled nutrients driven by estuarine circulation influences the timing and magnitude of phytoplankton blooms in semi-enclosed systems (Malone et al., 1988; Sugimoto et al., 2010). Thus, riverine nutrient inputs and the

entrainment of oceanic nutrients, which are both driven by freshwater flows, simultaneously regulate phytoplankton primary production (Tseng et al., 2014). However, the contribution of each nutrient source to phytoplankton production in open coastal systems influenced by oceanic water is largely unknown. Changes in the contribution from the fluxes could have complex effects on coastal phytoplankton production because the nutrient concentrations, composition, and volume of these two inputs can vary seasonally.

Tango Bay is an open bay in Japan that receives most of its riverine nutrient inputs from the Yura River (Fig. 1). Although the coastal zone of Tango Bay is relatively oligotrophic (Kasai et al., 2010; Watanabe et al., 2014), it provides important nursery grounds for many fish (Takeno et al., 2008; Islam et al., 2010). Although our previous study demonstrated that high river discharge enhanced primary production in Tango Bay (Watanabe et al., 2014), the mechanisms have not been examined quantitatively. Here we examined how freshwater flow affects phytoplankton dynamics in Tango Bay. First, we investigated the spatiotemporal distributions of physical parameters, nutrient concentrations, euphotic zone depth, and phytoplankton biomass (chlorophyll *a*). We then determined which nutrients [nitrogen (N), phosphorus (P), silica (Si) and iron (Fe)] limited phytoplankton growth using bioassays and stoichiometry. We also calculated riverine nutrient fluxes and the oceanic nutrients entrained by estuarine circulation. Finally, we compared seasonal fluctuations in phytoplankton biomass with nutrient fluxes and light availability to evaluate linkages between freshwater flow and coastal phytoplankton in this open bay.

2. Materials and methods

2.1. Study area

The Yura River has a total length of 146 km and a total catchment area of 1,880 km^2 (Fig. 1). Flow in the Yura River is variable (coefficient of variation [CV] = 1.27), with an annual variation that exceeds the world average (CV = 0.40; Finlayson and McMahon, 1988). Seasonal peaks in flow typically follow spring snowmelt and periods of high precipitation between May and July. Between August and December, precipitation is generally low. Tango Bay is a microtidal estuary with a spring tidal range of less than 0.5 m (Kasai et al., 2010). With an embayment degree of 0.9 (*ED* = the distance between the mouth and head of a bay/the width of the mouth), Tango Bay is more open than semi-enclosed bays in Japan (Hiroshima Bay: 2.6; Ise Bay: 3.6) and elsewhere (Chesapeake Bay: 16.3; San Francisco Bay: 19.5); accordingly, it is classified as an open bay.

2.2. Field surveys and sample analyses

Field surveys were conducted in the coastal zone of Tango Bay and in the downstream Yura River. Surveys in the coastal zone were conducted approximately every 10 days between December 2009 and July 2011 at four sampling stations with varying depths: T1, 5 m; T2, 10 m; T3, 20 m; T4, 30 m (Fig. 1). Additionally, three surveys were conducted at station T5 (depth: 50m) on 8 February, 22 March, and 26 April 2011 to assess the conditions of the deep zone in Tango Bay. To estimate riverine nutrient fluxes, surveys were conducted between May 2010 and July 2011 (n = 12) at station Y1, which was 16 km

upstream from the river mouth and was not influenced by seawater intrusion (Fig. 1 and Table 1). All surveys were conducted in the daytime and vertical profiles (every 0.1 m) of salinity, water temperature, chlorophyll fluorescence, and turbidity were measured at each station using a conductivity, temperature, and depth profiler (CTD; Compact-CTD; Alec Electronics, Kobe, Japan). Water samples for chlorophyll *a* (chl *a*) and nutrients were taken from the surface (depth: 0.2 m) and bottom (depth: 1.0 m above bottom) layers at each station in the coastal zone (T1–T5) and from the surface water at the river station (Y1). In addition, water samples for chl *a* and nutrients were taken from the middle layers between February and June 2011 (depth: T1, 2 m; T2, 2 and 5 m; T3, 2, 5 and 10 m; T4, 2, 5 and 15 m; T5, 2, 5, 10, and 25 m). All water samples were filtered through GF/F glass fiber filters (Whatman PLC, Maidstone, Kent, UK) prior to determination of chl *a* concentrations. The filters were then extracted in the dark in 90% acetone for 12 h, after which chl *a* concentrations were measured (Strickland and Parsons, 1972) using a calibrated fluorometer (Trilogy; Turner Designs, Sunnyvale, CA, USA). The vertical profile of chlorophyll fluorescence recorded by the CTD profiler was calibrated with the measured chl *a*. Chl *a* concentrations every 0.1 m were averaged vertically to calculate chl *a* concentrations for the entire water column. Water samples taken between March 2010 and July 2011 were used to determine nutrient concentrations [nitrate+nitrite (NO_x), phosphate (PO_4^{3-}), and dissolved silica (DSi)]. Water samples were filtered through a 0.45-μm mesh filter (Dismic filter; Advantec, Durham, NC, USA), after which nutrient concentrations were measured using a nutrient AutoAnalyzer (QuAAtro 2-HR; BL-Tec, Osaka, Japan) (Clesceri et al., 1998).

Potentially limiting nutrients were evaluated by comparing water nutrient ratios with elemental ratios in diatoms, which were the primary contributors to coastal phytoplankton production in Tango Bay during the study period (Watanabe, unpublished data). The elemental ratios in diatoms were estimated using the standard nutrient ratio (Redfield et al., 1963; Brzezinski, 1985) of N:P:Si = 16:1:16.

The daily mean global solar radiation (GSR) was obtained from the Japan Meteorological Agency based on measurements in Maizuru (Fig. 1). Daily mean river discharges (measured at Hami Bridge, 25 km upstream from the river mouth) and daily mean surface water temperatures (measured at Shimoamatsu, 31 km upstream from the river mouth) in the Yura River were obtained from the Ministry of Land, Infrastructure, Transport and Tourism and from the Meteorological Agency, respectively.

2.3. Bioassays

Bioassays were conducted on four sampling dates to determine the nutrients that potentially limited natural coastal phytoplankton assemblages. Water samples were taken from the chlorophyll maximum layer at station T4 on 23 February (depth: 10 m), 15 March (6 m), 9 May (17 m), and 23 June 2011 (20 m) using an iron-free Van Dorn water sampler. Water samples were collected in surface contamination clean (SCC) bottles (AS ONE, Osaka, Japan). Each sample (100 mL) was gently filtered through a 100-µm mesh net into a new SCC bottle (AS ONE).

To prevent iron contamination, all equipment and containers were immersed in 4 M HCl for at least 24 h and thoroughly rinsed with pure water (Milli-Q Water; Millipore, Billerica, MA, USA). In addition,

micropipette tips and bottles of stock solutions were washed in boiling 1 M nitric acid, hydrochloric acid, and Milli-Q water in that order. The following nutrients were added to the bottles individually and in all combinations: +N (nitrate: 200 µM final concentration), +P (phosphate: 10 µM), +Si [silicate: 33 µM] and +Fe (EDTA-chelated Fe: 0.2 µM). Although these concentrations are much higher than natural concentrations, they would not alter evaluation of the limiting nutrient. Controls were established by adding the same amount (1 mL) of pure water (Milli-Q water; Millipore). Three subsamples were dispensed into 10 mL acid-washed polystyrene tubes by acid-washed micropipettes in a clean air bench, which were incubated under a 14:10 light–dark cycle (100–120 µmol photons $m^{-2} s^{-1}$) at 15°C. The tubes were shaken once a day. The tubes were then analyzed for *in vivo* chlorophyll fluorescence (10-AU 005; Turner Designs) every few days over a 7–10-day time course, during which time the chlorophyll fluorescence of all subsamples became saturated. Although a bottle effect could bias the results of this long-term experiment (Hammes et al., 2010), such effects would not alter evaluation of the limiting nutrient. The rate of phytoplankton growth was calculated as the increase in fluorescence per day. Significant differences among treatment means were identified by one-way analysis of variance (ANOVA) followed by Tukey's honestly significant difference (HSD) test at $p<0.05$ using R 3.3.1 (R Core Team, 2016).

2.4. Estimation of riverine nutrient fluxes

Nutrient concentrations used for the estimation were obtained from 12 samplings of the surface

water at station Y1 (Fig. 1; Kasai et al., 2010). NO_x concentrations did not exhibit seasonal changes and were not significantly correlated with either water temperature or daily river discharge (Table 1; Spearman's rank correlation: $p>0.05$); therefore, the NO_x flux was calculated from the annual average concentration. In contrast, because of the significant linear relationship between PO_4^{3-} and DSi and water temperature (Table 1; Spearman's rank correlation: $r_s = 0.90$, $p<0.01$ and $r_s = 0.65$, $p<0.05$, respectively) the daily concentrations of PO_4^{3-} and DSi were calculated with linear models as follows:

$$C_P(T) = 0.0319 \times T + 0.381,$$

$$C_{Si}(T) = 2.07 \times T + 112,$$

where T, $C_P(T)$, and $C_{Si}(T)$ indicate the daily mean temperature and the concentrations (μM) of PO_4^{3-} and DSi, respectively. The nutrient flux equations were as follows:

$$NO_x \text{ flux} = C_N \times Q_f, \quad (R^2 = 0.96, n = 12),$$

$$PO_4^{3-} \text{ flux} = C_P(T) \times Q_f, \quad (R^2 = 0.97, n = 12),$$

$$\text{DSi flux} = C_{Si}(T) \times Q_f, \quad (R^2 = 0.94, n = 12),$$

where Q_f is the daily river discharge and C_N is the annual average concentration of NO_x at station Y1 (46 μM). Values of R^2 above 0.94 indicate that the models account for more than 94% of the fluctuations in the flux as measured in 12 surveys. However, during periods when the river discharge is higher than 250 m^3 s^{-1} there would be model uncertainty associated with estimations of the nutrient fluxes.

2.5. Estimation of the entrainment fluxes of nutrients using a box model

In this study, entrainment was defined as the transport of water and nutrients driven only by estuarine circulation. The flux of entrainment water was estimated using a box model (a salinity conservative model) that determined the entrained fluxes of nutrients from the offshore into the coastal zone. The coastal box was defined as the area shallower than 30 m, excluding Maizuru Bay (Fig. 1). The offshore box was defined as the zone deeper than 30 m. The halocline, which occurs at levels shallower than 5 m throughout most of the year, defined the coastal zone boxes as the surface layer above 5 m (box-1) and the deeper layer (box-2). The salinity conservative model was defined as:

$$V_1 \frac{\mathrm{d}S_1}{\mathrm{d}t} = Q\overline{S_2} - (Q + Q_f)\overline{S_1},$$

where Q, Q_f, and V_1 (1.35×10^8 m^3) represent the monthly flux of entrained water, the monthly freshwater flux (river discharge), and the volume of box-1, respectively; S_1 and S_2 are the spatial and vertical mean salinities of box 1 and box 2, and $\overline{S_1}$ and $\overline{S_2}$ are the monthly averages of S_1 and S_2, respectively. The flux of entrained water (Q) was estimated over monthly time steps.

Monthly nutrient fluxes driven by estuarine circulation were calculated by multiplying Q by the monthly mean nutrient concentrations in the bottom water at station T4. This model did not evaluate the impact of nutrient input from Maizuru Bay.

2.6. Estimation of the euphotic zone depth

The depth of the euphotic zone was estimated from turbidity data collected in the Tango Bay

coastal zone. First, we calculated the actual extinction coefficients (k, m^{-1}) using vertical profiles of the photosynthetic photon flux density (PPFD), measured by a PPFD meter (MDS MkV-L; Alec Electronics, Kobe, Japan). The PPFD was measured 13 times between December 2009 and September 2010 at stations T1–T4. Actual k values were calculated for both the surface layer (0–1 m) and the lower layer (>1 m) on 22 December 2009 and 1 March 2010 when high turbidity river plumes were observed. Actual k values were calculated for the whole water column on the other dates. To estimate the k value from turbidity, we modeled the data using a generalized linear model (GLM) with an identity link. A GLM allows the error distribution to be specified. We used a gamma distribution because the k values were strictly non-negative. The GLM equation was as follows (Fig. S1 and Table S1):

$$k = 0.1084 \times \text{Turbidity} + 0.1619.$$

The k value was calculated for both the surface layer (k_S; 0–1 m) and the lower layer (k_L; >1 m) on each sampling day. The euphotic zone depth (D_E, m) and the difference between the water depth (D, m) and D_E (ΔD_E) were calculated as follows:

$$D_E = -(\ln(0.01) + k_S - k_L) / k_L,$$

$$\Delta D_E = D - D_E.$$

The pseudo R^2 for the GLM was 0.88, calculated following the method outlined by McFadden (1973). The statistical analyses were conducted with R 3.3.1 (R Core Team, 2016).

2.7. Statistical analysis

We used a GLM with a gamma distribution and identity link to examine the effect of the riverine nutrient flux, nutrient flux driven by estuarine circulation, and D_E on the seasonal fluctuations in chl *a* as follows:

$$\overline{chl} = \overline{N_R} + \overline{N_O} + \overline{D_E} \text{ (full model),}$$

where $\overline{chl}$, $\overline{N_R}$, $\overline{N_O}$, and $\overline{D_E}$ indicate the monthly mean values of the water column chl *a* concentration, riverine NO_x flux, NO_x flux driven by estuarine circulation, and D_E, respectively. We selected the best model using downward stepwise model selection according to the Akaike Information Criterion (AIC; Akaike 1974). The statistical analyses were conducted in R 3.3.1 (R Core Team, 2016).

3. Results

3.1. Temporal change in biogeochemical parameters

Sea surface temperature peaked (29.5°C) in August 2010, when water in Tango Bay was stratified (Fig. 2a), then declined to ~10°C in February and March, when the water column was vertically mixed. Horizontally-averaged surface salinity ranged from 12.7 to 33.8, and decreased between February and April 2010, June and July 2010, September and October 2010, and February and April 2011 (Fig. 2b). Seasonal changes in bottom salinity were small, varying between 32.5 in summer and ~34 from March to June. Surface nutrient concentrations were high during periods of low salinity (March–April, June–July and September–October 2010 and February–April 2011; Fig. 2c–e). At salinities <30, NO_x, PO_4^{3-} and DSi

concentrations were often above 5, 0.2 and 20 μM, respectively. Bottom nutrient concentrations were high from December to February (Fig. 2c–e), with maximum NO_x, PO_4^{3-} and DSi concentrations reaching more than 3, 0.3 and 10 μM, respectively. Surface chl *a* concentrations were high between August and September (Fig. 2f), whereas bottom chl *a* concentrations were high between February and April in both 2010 and 2011. Column chl *a* concentrations were consistent with those in the bottom, and highest (>3 μg L^{-1}) between February and April in both 2010 and 2011 (Fig. 2g) and relatively low (~3 μg L^{-1}) between May and January, except November 2010.

There were temporal fluctuations in turbidity (Fig. 3a–d) with a maximum value of more than 50 FTU at the surface of station T1 (Fig. 3a). Turbidity was higher at the shallower stations (e.g., stations T1 and T2). The value of ΔD_E was generally lower than 0 m at stations T1 and T2 (Fig. 3e, f), and was higher than 0 m on 13 April 2010, when the surface turbidity increased dramatically because of river runoff; however, ΔD_E was generally controlled by the turbidity of the lower layer and increased close to 0 m from November to January (Fig. 3e, f). Values of ΔD_E ranged from −5.7 to 11.1 m and increased from November to January at station T3 (Fig. 3g). The value of ΔD_E remained higher than 0 m through the year at station T4 and only fluctuated slightly (Fig. 3h).

The chlorophyll maximum occurred at a depth of ~10 m between February and April in 2010 and 2011, although chl *a* concentrations were higher in 2011 than in 2010 (Fig. 4a, b). The vertical and temporal distributions of both temperature and salinity were similar between in 2010 and 2011 (Fig. 4c–f). Surface NO_x concentrations were highest with low salinity when river runoffs occurred (Fig. 4g, h). NO_x

concentrations in the middle and bottom layers were high in January and February, but decreased from March to April (Fig. 4g, h). The first peak in the chl *a* concentrations coincided with the increase in GSR in late March 2010 and early February 2011 (Fig. 4i, j). Values of ΔD_E decreased from December to March in both 2010 and 2011 (Fig. 4k, l) but increased to more than 0 m in late March 2010 (Fig. 4k).

The chlorophyll maximum was distributed in the shallow zone (~30 m) of Tango Bay between February and April in 2011 (Fig. 5a–c). Chl *a* concentrations were high at depths of 5–20 m. Salinity was low in surface waters (Fig. 5d–f). NO_x concentrations were generally high in surface waters (Fig. 5g–i). Bottom NO_x concentration was high in February 2011 and decreased in March and April 2011.

3.2. Coastal water nutrient ratios

Coastal water nutrient ratios (log-scale) are compared with the Redfield ratio in Fig. 6. In this study, N was defined as NO_x, P was defined as PO_4^{3-}, and Si was defined as DSi. The lines showing the Redfield ratio (N:P:Si = 16:1:16) delimited three areas, each characterized by potentially limiting nutrients. N/Si ratios were lower than 1 throughout the year in both surface and bottom waters (Fig. 6), indicating Si was not the limiting factor. N/P ratios in bottom water were lower than 16 throughout the year, but were often higher than 16 in surface water. N/P ratios were higher than 1 throughout the water column during the pre-blooming period (November–January) (Fig. 6a), but were often lower than 1 between February and July in bottom water (Fig. 6b, c) and between August and October in surface water (Fig. 6d).

3.3. Bioassay experiments

The rate of phytoplankton growth was significantly higher in the +P treatment than in the other groups in February, indicating that P was a potentially limiting nutrient (Fig. 7a–c). N was potentially limiting in March and May (Fig. 7d–i) In June, both N and P caused growth rates to increase significantly, indicating that both were potentially limiting nutrients (Fig. 7j, k).

3.4. Nutrient fluxes into the coastal zone

The median river discharge was 48 m^3 s^{-1} during the study period (Fig. 8a). River discharge was high from February to April because of melting snow. Additionally, sudden floods occurred between May and July, with the highest discharge recorded following two typhoons in May 2011. River discharge was generally low from summer to autumn, when there was little precipitation.

Following patterns of river discharge, NO_x, PO_4^{3-} and DSi fluxes from the Yura River into the coastal zone were high throughout February–April in both years (Fig. 8b–d) and remained high between May and July, with maximum values occurring in May 2011 (NO_x: 24.4 Mg [mega gram]-N day^{-1}; PO_4^{3-}: 0.99 Mg-P day^{-1}; DSi: 150.4 Mg-Si day^{-1}). Nutrient fluxes were low from August to January in 2010 (Fig. 8b–d).

The entrained water flux ranged from 81 × 10^6 to 416 × 10^6 m^3 day^{-1} (mean value: 157 × 10^6 m^3 day^{-1}), and the maximum estimated flux occurred in May 2011, when there were large floods (Fig. 8e). The entrained water flux was high from February to July, low from August to January and was

significantly related to the volume of river discharge (Pearson's correlation coefficient: r = 0.89, p<0.001; regression slope = 9.1). The ratio was comparable with previous estimates reported in coastal bays of Japan (Ise Bay: Q/Q_f = 2.5–30, Fujiwara et al., 1996; Hiroshima Bay: mean Q/Q_f = 7, Yamamoto et al., 2000).

The entrained flux of NO_x driven by estuarine circulation was higher from December to April (mean ± SD = 5.3 ± 3.5 Mg-N day^{-1}) than from May to October (1.0 ± 0.8 Mg-N day^{-1}) (Fig. 8f). The entrained fluxes of PO_4^{3-} and DSi were also higher from December to April (1.5 ± 0.7 Mg-P day^{-1}, 33.1 ± 15.2 Mg-Si day^{-1}) than from May to October (1.1 ± 0.6 Mg-P day^{-1}, 29.3 ± 17.3 Mg-Si day^{-1}) (Fig. 8g, h). Seasonal variations in the fluxes of PO_4^{3-} and DSi were smaller (CVs of 0.52 and 0.51, respectively) than in those of NO_x (CV = 1.02).

Maizuru Bay is another potential source of nutrients to Tango Bay; however, this nutrient input (~0.1 Mg-N day^{-1}; Miwa and Ikeno, 2008) was one order of magnitude lower than the riverine nutrient fluxes from Yura River and the entrained fluxes of nutrients (Fig. 8).

The model selection results for seasonal fluctuations in chl *a* in the water column supported the effects of the entrained flux of NO_x and D_E with a 1-month time lag (Table 2). The model that had the lowest AIC value for the 1-month time lag also included the riverine NO_x flux; however, the Δ_i and ω_i values of the model were similar to those of the $\overline{N_O} + \overline{D_E}$ model. The model with the lowest AIC value for the 0-month time lag also included the entrained flux of NO_x and D_E, but six models (including a null model) had similar values of Δ_i and ω_i (Table 2).

4. Discussion and conclusions

4.1. Nutrient limitation of coastal phytoplankton

Spatiotemporal changes in nutrient concentrations show that seasonal patterns in nutrient limitation are affected by both the freshwater inflow and the entrainment of oceanic water in Tango Bay. Between November and January, nutrient concentrations were higher than the average half saturation concentration (K_s) required for phytoplankton uptake (1.0 μM dissolved inorganic N, 0.2 μM PO_4^{3-}, and 2.0 μM DSi) (Dortch and Whitledge, 1992). Nutrient ratios during this time were also similar to the Redfield ratio (Fig. 6), indicating that nutrient levels were not potential limits on primary production.

Nutrient consumption by blooming phytoplankton leads to severe nutrient depletion in late spring (Figs. 2, 4, and 5). The nutrient supply from the deeper zone (>50 m) also decreased after April owing to the weakening of vertical mixing (Fig. 5g–i; Kim et al., 2012). NO_x and PO_4^{3-} concentrations were below the average K_s in April; thus, phytoplankton growth would have been potentially limited by both nutrients during this period (Fig. 2c, d). The increased phytoplankton growth with the simultaneous supply of N and P in bioassays (Fig. 7a–f) supported this conclusion.

Both NO_x and PO_4^{3-} in the bottom water decreased below the average K_s between May and October (Fig. 2c, d), indicating severely nutrient-limited conditions (Figs. 6 and 7g–l). Chl *a* concentrations were high in a thin surface layer in summer (Fig. 2f); however, this accumulated phytoplankton was occupied by freshwater phytoplankton flowing out of the river (Watanabe et al., 2014; Watanabe, unpublished data), and would not contribute to the coastal phytoplankton production (Fig. 2g).

To examine how NH_4^+ affected nutrient limitation, we conducted stoichiometric analysis using the NH_4^+ concentration data from July 2007 to March 2008 (Watanabe et al., 2014). The spatiotemporal changes in potentially limiting nutrients (Fig. S2) were similar to the results in Fig. 6; i.e., N and P were potential limits in the bottom and surface waters, respectively. However, the N/P and N/Si ratios became closer to the Redfield ratio, suggesting that the NH_4^+ supply (e.g., riverine inputs and recycling in the coastal zone) might temporarily buffer the N limiting condition.

4.2. Effects of nutrient fluxes and light availability on seasonal fluctuations in phytoplankton

Oceanic nutrients entrained via estuarine circulation fuel coastal phytoplankton production in Tango Bay, which has been shown also in other open coastal systems (Davis et al., 2014). Results from the GLMs supported an increase in the water column chl *a* with increases in both $\overline{N_O}$ and $\overline{D_E}$ with a 1-month time lag, and, in turn, did not support any influence of $\overline{N_R}$, $\overline{N_O}$, and $\overline{D_E}$ with the 0-month time lag (Table 2). The 1-month time lag between the observed increases in the NO_x flux and chl *a* concentrations indicates that phytoplankton blooms start approximately 1 month after increases in the NO_x inflows in estuarine circulation (Figs. 2g, 4a, b, and 8f). This time lag may be caused by other limiting factors, such as light availability (Figs. 3 and 4i–l; Shiozaki et al., 2014; Saba et al., 2015).

Seasonal changes in the depth of the euphotic zone also influence coastal phytoplankton in Tango Bay (Table 2). The depth of the euphotic zone decreased from November to January, especially at shallow stations (e.g., station T1 and T2), and these decreases were not related to river runoff. The northwesterly

wind induced by the winter monsoon is an important forcing component for the Sea of Japan and Tango Bay (Itoh et al., 2016). The shoaling of the euphotic zone depth with increases in turbidity may be caused by wind events in winter, and may have inhibited phytoplankton production during the nutrient-rich period (November–January).

The influence of riverine NO_x fluxes on seasonal changes in chl *a* concentrations in Tango Bay was poorly supported by the GLM outputs (Table 2). Nutrients in the river plume would not be used efficiently by coastal phytoplankton despite the sufficient light availability in the surface waters (Fig. 3). Riverine nutrients are efficiently transported offshore because of the microtidal conditions in Tango Bay, resulting in low availability of riverine nutrients to phytoplankton in the shallow coastal zone (<30 m). Davis et al. (2014) also found that terrestrial nutrients played only a minor role in an open coast phytoplankton assemblage.

Our results show that, during late spring and summer, the entrained low-nutrient seawater dilutes nutrient-replete freshwater and reduces primary production in this open bay. This dilution effect is illustrated by the nutrient and phytoplankton dynamics observed after the typhoons in May 2011, i.e., the high river discharge caused by the typhoons supplied large amounts of riverine nutrients (Fig. 8a–d) but entrained low-nutrient seawater from offshore (Fig. 8e–h), which induced low-nutrient and low-chlorophyll conditions (Fig. 2b–g). In turn, in semi-enclosed bays, the entrained water is nutrient-rich and supports phytoplankton growth year round because sedimentary organic matter is mineralized, increasing nutrient concentrations (Yamamoto et al., 2000; Sugimoto et al., 2010; Cloern et al., 2014).

Thus, the relationship between freshwater flow and coastal primary production depends on the embayment degree (*ED*).

4.3. Drivers of phytoplankton blooms in winter and spring

Phytoplankton blooms in Tango Bay occurred between February and April in 2010 and 2011 (Figs. 2f, g, and 4a, b), as well as in other years (Kasai et al., 2010; Watanabe et al., 2014). However, riverine discharge transports surface phytoplankton offshore, resulting in low surface chl *a* concentrations despite the nutrient-rich conditions and in the maximum chl *a* values occurring in the middle layers (5–20 m).

The timing of the bloom matched that of increases in GSR and an increase in D_E, suggesting that light would limit phytoplankton growth from December to February, despite nutrient-replete conditions (Fig. 4). Phytoplankton blooms under nutrient-limited conditions between March and April would be supported by additional nutrient inputs. These increases in phytoplankton biomass coincided with floods (river discharge >100 $m^3 s^{-1}$), suggesting that the freshwater flow drives oceanic nutrient inflows in spring. Recycled nutrients in Tango Bay could fuel the bloom during late spring, when the entrained flux of nutrients from the offshore declines because of weakened vertical mixing (Fig. 5i).

The dilution effect of estuarine circulation (Yamamoto et al., 2000; Harrison et al., 2008; Artigas et al., 2014) would create the nonlinear relationship between freshwater flux and blooms. The magnitude of the phytoplankton bloom was smaller in 2010 than in 2011 (Figs. 2f and 4a, b), while the entrained water flux was ~1.6 times larger in 2010 than in 2011 (Fig. 8e). The occurrence of shoaling of the euphotic zone

would also inhibit phytoplankton production in March 2010 (Fig. 4k, l). However, other physical and biogeochemical factors (e.g., phytoplankton species composition, top-down effect of herbivores, wind, tide, and oceanic currents) should be assessed in future studies.

4.4. Influence of primary production on higher trophic levels in Tango Bay

Phytoplankton blooms from winter to early spring are mainly fueled by the entrainment of oceanic nutrients in Tango Bay. The biomass of secondary producers also increases during the blooms (Watanabe et al., 2014; Akiyama et al., 2015), which may regulate phytoplankton production via top-down control. Moreover, flounder and temperate seabass larvae and juveniles settle in the coastal zone during times of high production of their prey organisms (Takeno et al., 2008; Islam et al., 2010). When coastal phytoplankton production is limited by nutrients from late spring to summer, some juvenile temperate seabass migrate into the river, where the high abundance of prey enhances their growth relative to individuals remaining in the shallow coastal zone (Fuji et al., 2011; Fuji et al., 2014; Watanabe et al., 2014). These fish rely on seasonal fluctuations in both freshwater flow and coastal conditions (e.g. vertical mixing and wind events) that determine the dynamics of their prey.

Acknowledgments

This study was partly supported by the Coastal Ecosystem Complex Project of the Ocean Resource Use Promotion Technology Development Program, MEXT of Japan. We are grateful to K. Sato, S. Akiyama, S.

Matsui-Akiyama, T. Fuji, and T. Funahashi for their help with the sampling. We express special thanks to M. Heidarzadeh, K. Suzuki, K. Minami, and K. Takahashi for their valuable comments.

References

Akaike, H., 1974. A new look at the statistical model identification. IEEE Trans Automat Contr 19, 716–723.

Akiyama, S., Ueno, M., Yamashita, Y., 2015. Population dynamics and reproductive biology of the mysid *Orientomysis japonica* in Tango Bay, Japan. Plankton Benthos Res. 10, 121–131.

Artigas, M.L., Llebot, C., Ross, O.N., Neszi, N.Z., Rodellas, V., Garcia-Orellana, J., Masqué, P., Piera, J., Estrada, M., Berdalet, E., 2014. Understanding the spatio-temporal variability of phytoplankton biomass distribution in a microtidal Mediterranean estuary. Deep Sea Res. II 101, 180–192.

Brzezinski, M.A., 1985. The Si:C:N ratio of marine diatoms: interspecific variability and the effect of some environmental variables. J. Phycol. 21, 347–357.

Caddy, J.F., Bakun, A., 1994. A tentative classification of coastal marine ecosystems based on dominant processes on nutrient supply. Ocean Coast. Manag. 23, 201–211.

Clesceri, L.S., Greenberg, A.E., Eaton, A.D., 1998. Standard Methods for the Examination of Water and Wastewater. APHA, AWWA, and WEF, Maryland.

Cloern, J.E., 1996. Phytoplankton bloom dynamics in coastal ecosystems: A review with some general lessons from sustained investigation of San Francisco Bay, California. Rev. Geophys. 34, 127–168.

Cloern, J.E., Foster, S.Q., Kleckner, A.E., 2014. Phytoplankton primary production in the world's estuarine-coastal ecosystems. Biogeosciences 11, 2477–2501.

Cloern, J.E., Jassby, A.D., 2008. Complex seasonal patterns of primary producers at the land–sea interface. Ecol. Lett. 11, 1294–1303.

Connolly, R.M., Schlacher, T.A., Gaston, T.F., 2009. Stable isotope evidence for trophic subsidy of coastal benthic fisheries by river discharge plumes off small estuaries. Mar. Biol. Res. 5, 164–171.

Davis, K.A., Banas, N.S., Giddings, S.N., Siedlecki, S.A., MacCready, P., Lessard, E.J., Kudela, R.M., Hickey, B.M., 2014. Estuary-enhanced upwelling of marine nutrients fuels coastal productivity in the U.S. Pacific Northwest. J. Geophys. Res. Oceans 119, 8778–8799.

Dortch, Q., Whitledge, T.E., 1992. Does nitrogen or silicon limit phytoplankton production in the Mississippi River plume and nearby regions? Continent. Shelf Res. 12, 1293–1309.

Finlayson, B.L., McMahon, T.A., 1988. Australia vs the world: A comparative analysis of stream flow characteristics. In Warner, R.F. (Eds.), Fluvial Geomorphology of Australia. Academic Press, Sydney, pp. 17–40.

Fuji, T., Kasai, A., Suzuki, K.W., M. Ueno, Yamashita, Y., 2011. Migration ecology of juvenile temperate seabass *Lateolabrax japonicus*: a carbon stable-isotope approach. J. Fish. Biol. 78, 2010–2025.

Fuji, T., Kasai, A., Ueno, M., Yamashita, Y., 2014. Growth and migration patterns of juvenile temperate seabass *Lateolabrax japonicus* in the Yura River estuary, Japan—combination of stable isotope ratio and otolith microstructure analyses. Environ. Biol. Fish. 97, 1221–1232.

Fujiwara, T., Fukui, S., Sugiyama, Y., 1996. Seasonal variation in stratification and estuarine circulation of Ise Bay. Oceanogr. Japan 5, 235–244. (in Japanese with English abstract)

Hammes, F., Vital, M., Egli, T., 2010. Critical evaluation of the volumetric “bottle effect” on microbial batch growth. Appl. Environ. Microbiol. 76, 1278–1281.

Harrison, P.J., Yin, K., Lee, J.H.W., Gan, J., Liu, H., 2008. Physical–biological coupling in the Pearl River Estuary. Continent. Shelf Res. 28, 1405–1415.

Islam, M.S., Ueno, M., Yamashita, Y., 2010. Growth-dependent survival mechanisms during the early life of a temperate seabass (*Lateolabrax japonicus*): field test of the ‘growth-mortality’ hypothesis. Fish. Oceanogr. 19, 230–242.

Itoh, S., Kasai, A., Takeshige, A., Zenimoto, K., Kimura, S., Suzuki, K.W., Miyake, Y., Funahashi, T., Yamashita, Y., Watanabe, Y., 2016. Circulation and haline structure of a microtidal bay in the Sea of Japan influenced by the winter monsoon and the Tsushima Warm Current. J. Geophys. Res. Oceans 121, 6331–6350.

Kasai, A., Kurikawa, Y., Ueno, M., Robert, D., Yamashita, Y., 2010. Salt-wedge intrusion of seawater and its implication for phytoplankton dynamics in the Yura Estuary, Japan. Estuar. Coast. Shelf. Sci. 86,408–414.

Kim, D., Yang, E.J., Kim, K.H., Shin, C.-W., Park, J., Yoo, S., Hyun, J.-H., 2012. Impact of an anticyclonic eddy on the summer nutrient and chlorophyll *a* distributions in the Ulleung Basin, East Sea (Japan Sea). ICES J. Mar. Sci. 69, 23–29.

Kimmerer, W.J., 2002. Physical, biological, and management responses to variable freshwater flow into the San Francisco Estuary. Estuaries 25, 1275–1290.

Kostecki C., Le Loc'h, F., Roussel, J.-M., Desroy, N., Huteau, D., Riera, P., Le Bris, H., Le Pape, O., 2010. Dynamics of an estuarine nursery ground: the spatio-temporal relationship between the river flow and the food web of the juvenile common sole (*Solea solea*, L.) as revealed by stable isotopes analysis. J. Sea Res. 64, 54-60.

McFadden, D., 1973. Conditional logit analysis of qualitative choice behavior. In Zarembka, P. (Eds.), Frontiers in Econometrics, Academic Press, New York, pp. 105–142.

Mallin, M.A., Paerl, H.W., Rudek, J., Bates, P.W., 1993. Regulation of estuarine primary production by watershed rainfall and river flow. Mar. Ecol. Progr. Ser. 93, 199–203.

Malone, T.C., Crocker, L.H., Pike, S.E., Wendler, B.W., 1988. Influences of river flow on the dynamics of phytoplankton production in a partially stratified estuary. Mar. Ecol. Progr. Ser. 48, 235–249.

Miwa, H., Ikeno, H., 2008. Numerical analysis of tidal current and water quality in stratified field on summer in Maizuru Bay. Ann. J. Hydraul. Eng. 52, 1387-1392. (in Japanese, with English Abstract)

Murrell, M.C., Hagy III, J.D., Lores, E.M., Greene, R.M., 2007. Phytoplankton production and nutrient distributions in a subtropical estuary: Importance of freshwater flow. Estuar. Coast. 30, 390–402.

Paerl, H.W., Rudek, J., Mallin, M.A., 1990. Stimulation of phytoplankton production in coastal waters by natural rainfall inputs: Nutritional and trophic implications. Mar. Biol. 107, 247–254.

R Core Team, 2016. R: A language and environment for statistical computing. R Foundation for Statistical

Computing, Vienna, Austria, URL. <https://www.R-project.org/>.

Redfield, A.C., Ketchum, B.H., Richard, F.A., 1963. The influence of organisms on the composition of the sea water. In Hill, M.N. (Eds), The Sea, Vol. 2. Wiley, New York, pp. 26–77.

Saba, V.S., Hyde, K.J.W., Rebuck, N.D., Friedland, K.D., Hare, J.A., Kahru M., Fogarty, M.J., 2015. Physical associations to spring phytoplankton biomass interannual variability in the U.S. Northeast Continental Shelf. J. Geophys. Res. Biogeosciences 120, 205–220.

Scharler, U.M., Baird, D., 2005. A comparison of selected ecosystem attributes of three South African estuaries with differing freshwater inflow regimes, using network analysis. J. Mar. Syst. 56, 283–308.

Shiozaki, T., Ito, S.-I., Takahashi, K., Saito, H., Nagata, T., Furuya, K., 2014. Regional variability of factors controlling the onset timing and magnitude of spring algal blooms in the northwestern North Pacific. J. Geophys. Res. Oceans 119, 253–265.

Smith Jr., W.O., Demaster, D.J., 1996. Phytoplankton biomass and productivity in the Amazon River plume: correlation with seasonal river discharge. Continent. Shelf Res. 16, 291–319.

Strickland, J.D.H., Parsons, T.R., 1972. A practical handbook of seawater analysis. Bull. Fish. Res. Board Canada 167, 201–203.

Sugimoto, R., Kasai, A., Miyajima, T., Fujita, K., 2010. Modeling phytoplankton production in Ise Bay, Japan: Use of nitrogen isotopes to identify dissolved inorganic nitrogen sources. Estuar. Coast. Shelf Sci. 86, 450–466.

Sugimoto, R., Kasai, A., Yamao, S., Fujiwara, T., Kimura, T., 2004. Variation in particulate organic matter

accompanying changes of river discharge in Ise Bay. Bull. Japan. Soc. Fish. Oceanogr. 68, 142–150. (in Japanese with English abstract)

Takeno, K., Hamanaka, Y., Okano, I., 2008. Differences in growth of young Japanese flounder *Paralichthys olivaceus* in two semi-enclosed bays of the Sea of Japan, Kyoto. Aquaculture Sci. 56, 513–522.

Tseng, Y.-F, Lin, J., Dai, M., Kao, S.-J., 2014. Joint effect of freshwater plume and coastal upwelling on phytoplankton growth off the Changjiang River. Biogeosciences 11, 409–423.

Watanabe, K., Kasai, A., Antonio, E.S., Suzuki, K., Ueno, M., Yamashita, Y., 2014. Influence of salt-wedge intrusion on ecological processes at lower trophic levels in the Yura Estuary, Japan. Estuar. Coast. Shelf Sci. 139, 67–77.

Yamamoto, T., Yoshikawa, S., Hashimoto, T., Takasugi, Y., Matsuda, O., 2000. Estuarine circulation process in the northern Hiroshima Bay, Japan. Bull. Coast. Oceanogr. 37, 111–118. (in Japanese with English abstract)

Figure captions

Fig. 1. Location of Tango Bay and the Yura River. Gray circles indicate coastal stations and the open circle is the river station. Distance from the river mouth to each coastal station: T1, 0.95 km; T2, 1.35 km; T3, 2.40 km; T4, 3.70 km; T5, 10.0 km. The shaded area depicts the coastal boxes used to calculate the entrained water flux driven by estuarine circulation. The closed circle marks the site where daily mean global solar radiation was monitored by the Japan Meteorological Agency in Maizuru

Fig. 2. Temporal changes in mean (**a**) temperature (°C), (**b**) salinity, (**c**) NO_x (μM), (**d**) PO_4^{3-} (μM), (**e**) DSi (μM), (**f**) chl *a* (μg L^{-1}) and (**g**) column chl *a* concentration (μg L^{-1}) of stations T1–T4 in Tango Bay. Red and blue circles indicate means of surface and bottom waters, respectively. The scales for the surface and bottom nutrient concentrations are different. Column chl *a* concentrations are water column means. Error bars indicate ±standard deviations of the mean values (n=4)

Fig. 3. Temporal changes in turbidity (FTU) at stations (**a**) T1, (**b**) T2, (**c**) T3 and (**d**) T4, and in ΔD_E (m) at stations (**e**) T1, (**f**) T2, (**g**) T3 and (**h**) T4. Red and blue circles indicate the surface (0–1 m) and lower layers (>1 m), respectively. ΔD_E is the difference between the water depth and the euphotic water depth, which was estimated with a generalized linear model using turbidity data

Fig. 4. Temporal variability (December–June 2010 and 2011) in (**a**, **b**) the vertical distribution of chl *a*

concentration, (**c**, **d**) the vertical distribution of temperature, (**e**, **f**) the vertical distribution of salinity, (**g**, **h**) NO_x concentration (μM), (**i**, **j**) global solar radiation (GSR), and (**k**, **l**) ΔD_E in Tango Bay. The parameters in (**a**–**h**, **k**, **l**) were measured at station T2. The solid gray and black line in (**i, j**) are the daily values and the 5-day moving averages of GSR, respectively. ΔD_E is the difference between the water depth and the euphotic water depth, which was estimated from the turbidity data by a generalized linear model

Fig. 5. Spatial distribution of (**a**–**c**) chl *a* concentration, (**d**–**f**) salinity, and (**g**–**i**) NO_x concentration on 8 February, 22 March, and 26 April 2011. Closed circles in (**g**–**i**) show each sampling depth for NO_x concentrations.

Fig. 6. N:P:Si molar ratios (log N/Si ratio vs. log N/P ratio) in the coastal waters of Tango Bay (**a**) from November to January, (**b**) from February to April, (**c**) from May to July, and (**d**) from August to October in 2010 and 2011. N, P and Si indicate NO_x, PO_4^{3-} and DSi, respectively. The potentially limiting nutrients in the three areas delimited by the Redfield ratio (N:P:Si = 16:1:16) are different. Open and closed circles indicate nutrient ratios in the surface and bottom water, respectively

Fig. 7. Effects of nutrient addition (N, P, Si, and Fe individually and all combinations) on the rate of phytoplankton growth at station T4 in (**a**–**c**) February, (**d**–**f**) March, (**g**–**i**) May and (**j**–**l**) June 2011. For each month, the potentially limiting nutrients are shown. Error bars indicate ±standard deviations of the

mean values (n=3). Mean growth rates among treatments (for each graph) were compared by one-way ANOVA followed by Tukey's HSD multiple comparison test. Significant differences (p<0.05) are indicated by different lowercase letters. NA: not analyzed

Fig. 8. Seasonal variation in (**a**) daily mean river discharge (m^3 s^{-1}), in monthly mean riverine flux of (**b**) NO_x (Mg [mega gram]-N day^{-1}), (**c**) PO_4^{3-} (Mg-P day^{-1}), and (**d**) DSi (Mg-Si day^{-1}), in the (**e**) entrained water flux (10^6 m^3 day^{-1}), (**f**) NO_x flux (Mg [mega gram]-N day^{-1}), (**g**) PO_4^{3-} flux (Mg-P day^{-1}), and (**h**) DSi flux (Mg-Si day^{-1}) driven by estuarine circulation (EC) in the Tango Bay shallow coastal zone. The riverine nutrient fluxes were estimated by the model from river discharge and temperature data. The entrained water flux was calculated with a box model. The nutrient fluxes driven by EC were estimated from the entrained water flux and the monthly mean nutrient concentrations in the bottom water at station T4. Error bars are standard deviations of the estimates. The dashed line in (**a**) shows the median river discharge over the entire study period

Table 1 River discharge, temperature, and nutrient concentrations of the surface water at station Y1, 16 km upstream from the river mouth

Survey	River discharge ($m^3\ s^{-1}$)	Temperature (°C)	NO_x (μM)	PO_4^{3-} (μM)	DSi (μM)
14 May 2010	34	15.2	44	1.0	131
11 Jun 2010	20	23.6	37	0.9	135
17 Jul 2010	143	22.3	38	0.9	181
13 Aug 2010	64	25.6	49	1.4	178
19 Aug 2010	22	29.6	53	1.6	188
18 Nov 2010	20	12.5	49	0.8	87
21 Jan 2011	44	4.8	47	0.6	128
19 Feb 2011	250	6.0	58	0.5	108
19 Mar 2011	95	7.4	40	0.6	166
25 Apr 2011	142	11.7	49	0.7	162
25 Jun 2011	52	24.8	39	0.9	136
26 Jul 2011	25	24.4	54	1.1	178

Table 2 Model selection results for riverine NO_x flux ($\overline{N_R}$), NO_x flux driven by estuarine circulation ($\overline{N_O}$), and the depth of the euphotic zone ($\overline{D_E}$) explaining seasonal change in the monthly mean values of the water column chl *a* concentrations. The estimated coefficient and the standard error (in parentheses) are shown for each explanatory variable. *df*, AIC, Δ_i, and ω_i indicate the degrees of freedom, the Akaike Information Criterion, AIC differences, and AIC weights, respectively. Models with small Δ_i (<2) are represented in this table. The 1-month time lag accounts for a 1-month delay in the chl *a* response to NO_x inputs and D_E changes. **, p<0.01

GLMs	$\overline{N_R}$	$\overline{N_O}$	$\overline{D_E}$	*df*	AIC	Δ_i	ω_i
1-month time lag							
$\overline{N_R}$ + $\overline{N_O}$ + $\overline{D_E}$	0.028 (0.023)	0.265 (0.074)**	0.082 (0.024)**	5	30.8	0.00	0.408
$\overline{N_O}$ + $\overline{D_E}$		0.241 (0.076)**	0.090 (0.027)**	4	31.0	0.17	0.375
0-month time lag							
$\overline{N_O}$ + $\overline{D_E}$		0.121 (0.081)	0.065 (0.040)	4	38.3	0.00	0.236
Null model				2	38.9	0.60	0.175
$\overline{N_O}$		0.084 (0.075)		3	39.0	0.67	0.169
$\overline{N_R}$ + $\overline{N_O}$ + $\overline{D_E}$	0.016 (0.034)	0.120 (0.085)	0.060 (0.041)	5	40.0	1.68	0.102
$\overline{N_R}$	0.073 (0.059)			3	40.0	1.76	0.098
$\overline{D_E}$			0.043 (0.051)	3	40.1	1.86	0.093

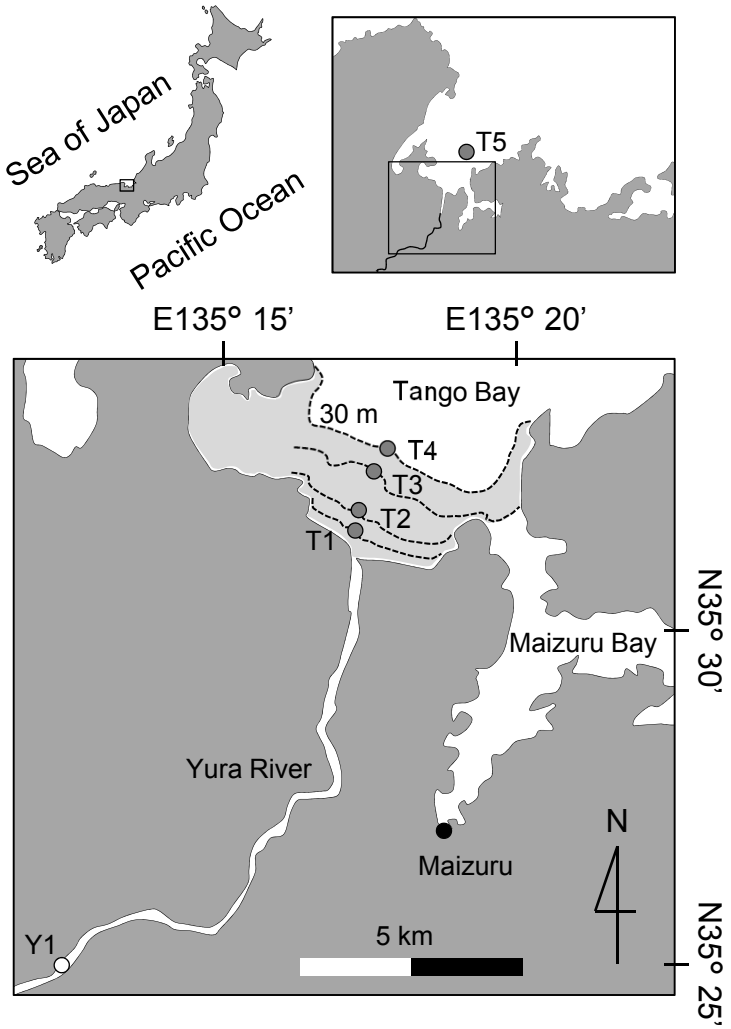
Sea of Japan
Pacific Ocean
T5
E135° 15'
E135° 20'
Tango Bay
30 m
T4
T3
T2
T1
Maizuru Bay
N35° 30'
Yura River
N
Maizuru
5 km
Y1
N35° 25'

FIG. 1

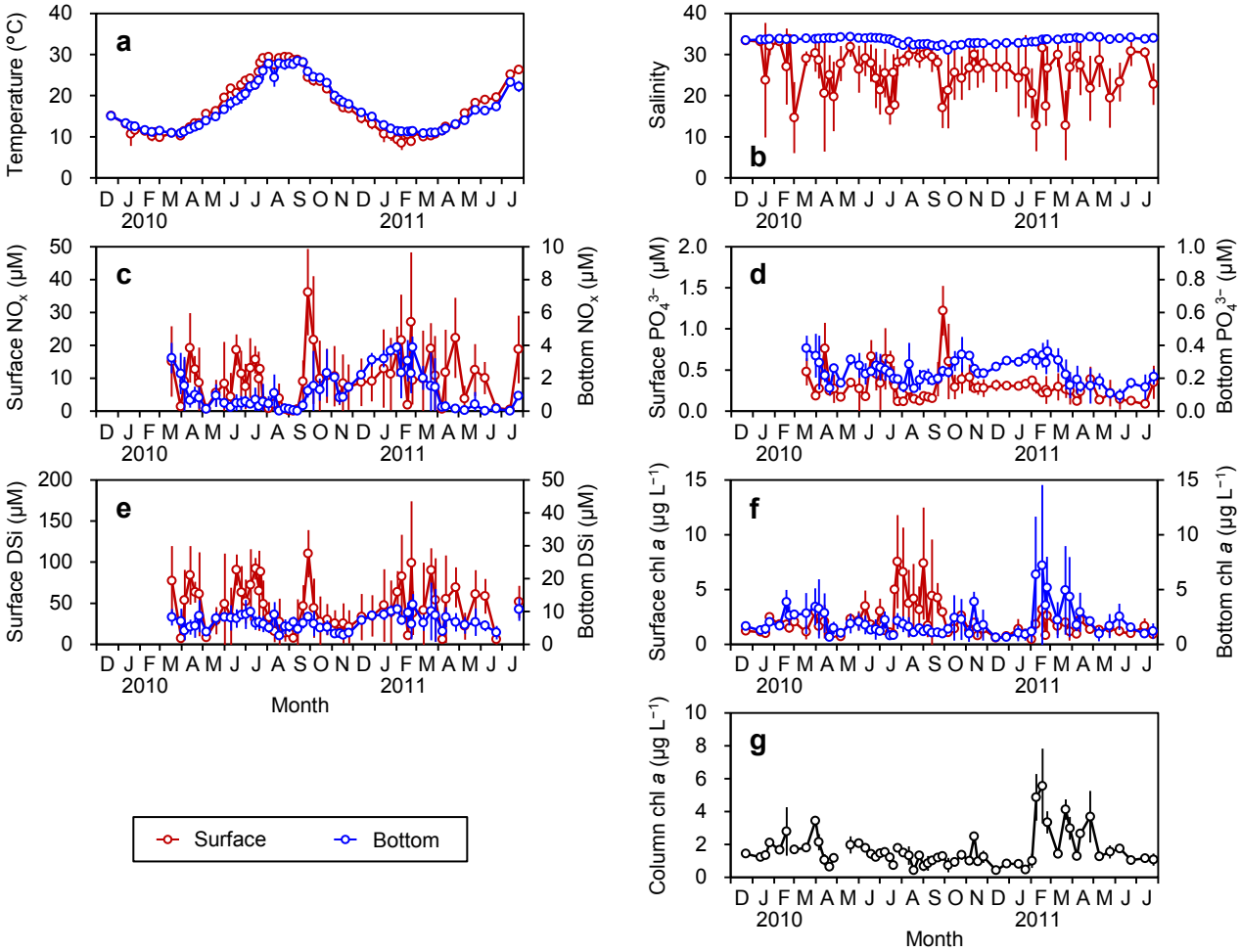
a
Temperature (°C)
b
Salinity
c
Surface NO_x (μM)
Bottom NO_x (μM)
d
Surface PO_4^{3-} (μM)
Bottom PO_4^{3-} (μM)
e
Surface DSi (μM)
Bottom DSi (μM)
f
Surface chl *a* (μg L^{-1})
Bottom chl *a* (μg L^{-1})
g
Column chl *a* (μg L^{-1})
D J F M A M J J A S O N D J F M A M J J
2010
2011
Month
Surface
Bottom

FIG. 2

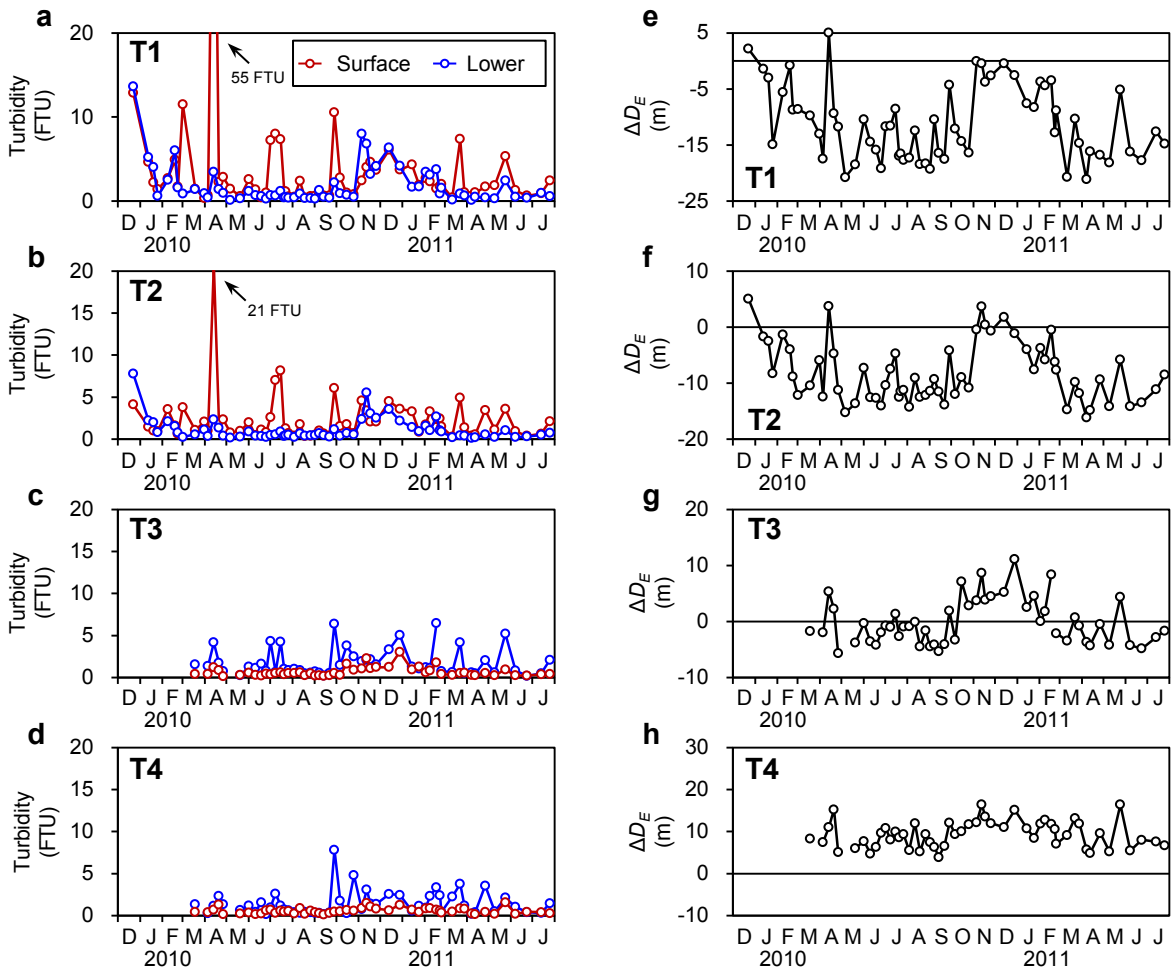
a
T1
55 FTU
Surface
Lower
Turbidity (FTU)
b
T2
21 FTU
c
T3
d
T4
e
T1
f
T2
g
T3
h
T4
ΔD_E (m)
D J F M A M J J A S O N D J F M A M J J
2010
2011

FIG. 3

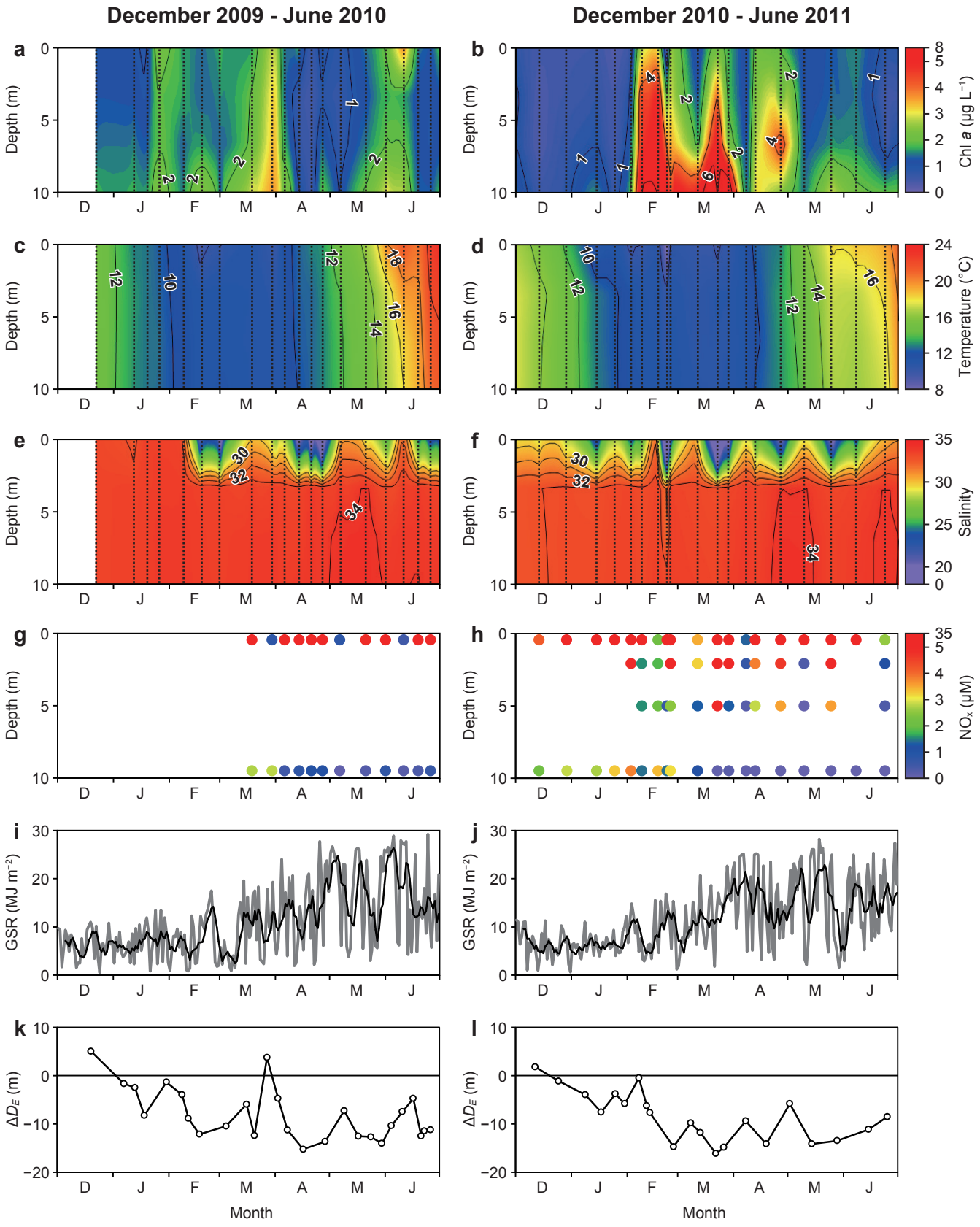
December 2009 - June 2010
December 2010 - June 2011
a
b
c
d
e
f
g
h
i
j
k
l
Depth (m)
Chl a (µg L⁻¹)
Temperature (°C)
Salinity
NOx (µM)
GSR (MJ m⁻²)
ΔDE (m)
D J F M A M J
Month

FIG 4

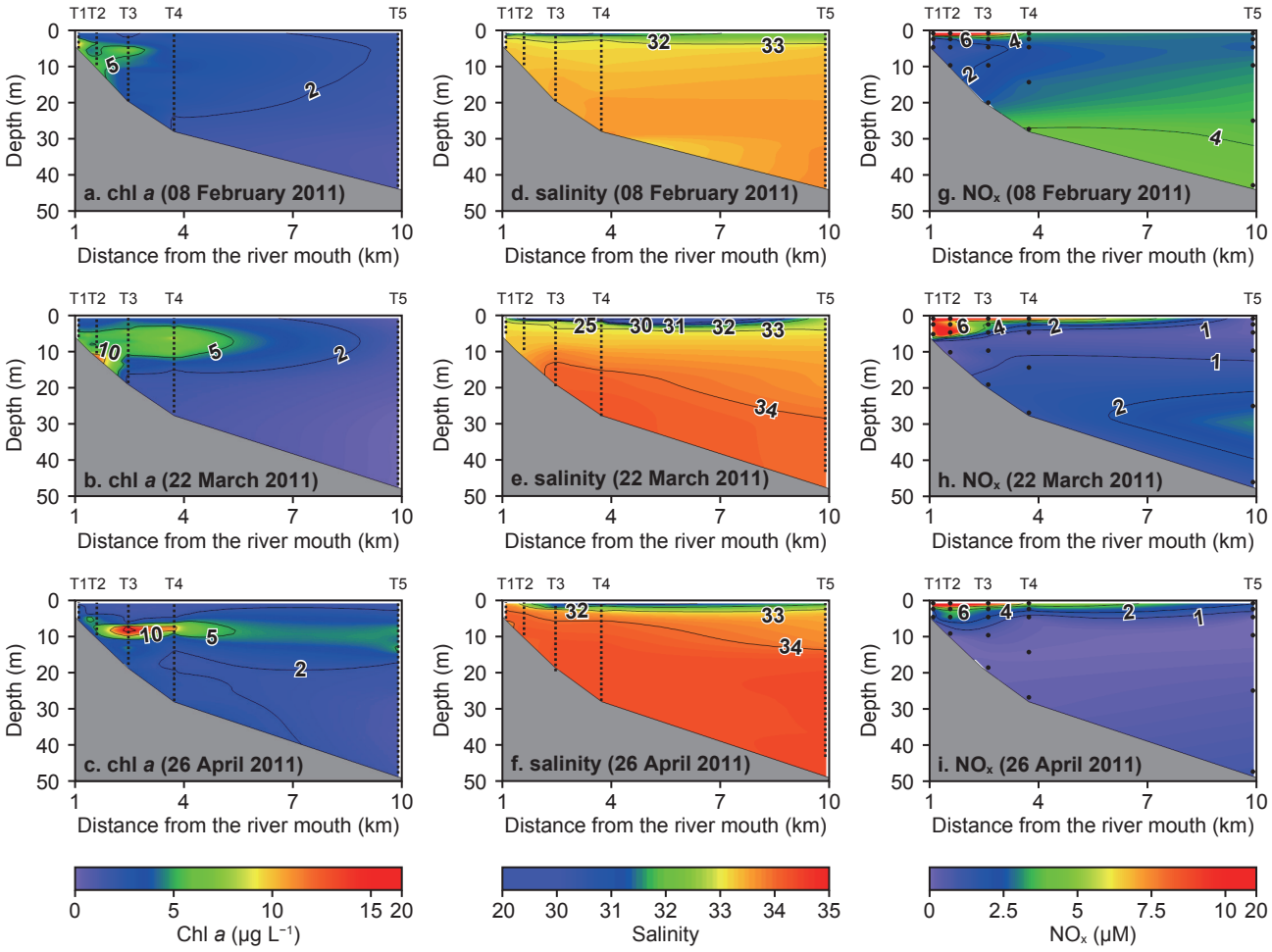
T1T2
T3
T4
T5
Depth (m)
Distance from the river mouth (km)
a. chl a (08 February 2011)
b. chl a (22 March 2011)
c. chl a (26 April 2011)
d. salinity (08 February 2011)
e. salinity (22 March 2011)
f. salinity (26 April 2011)
g. NOx (08 February 2011)
h. NOx (22 March 2011)
i. NOx (26 April 2011)
Chl a (µg L⁻¹)
Salinity
NOx (µM)

FIG 5

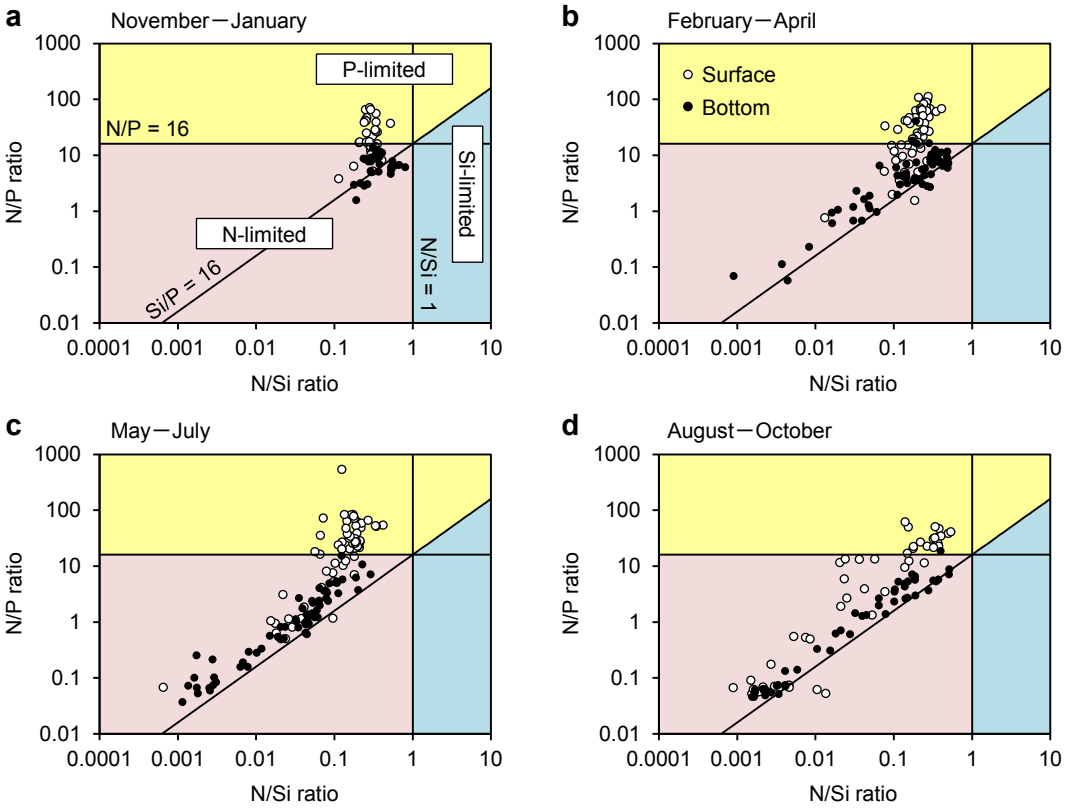
a
November—January
P-limited
N/P = 16
N-limited
Si/P = 16
Si-limited
N/Si = 1
N/P ratio
N/Si ratio
b
February—April
Surface
Bottom
c
May—July
d
August—October
1000
100
10
1
0.1
0.01
0.0001
0.001
0.01
0.1
1
10

FIG. 6

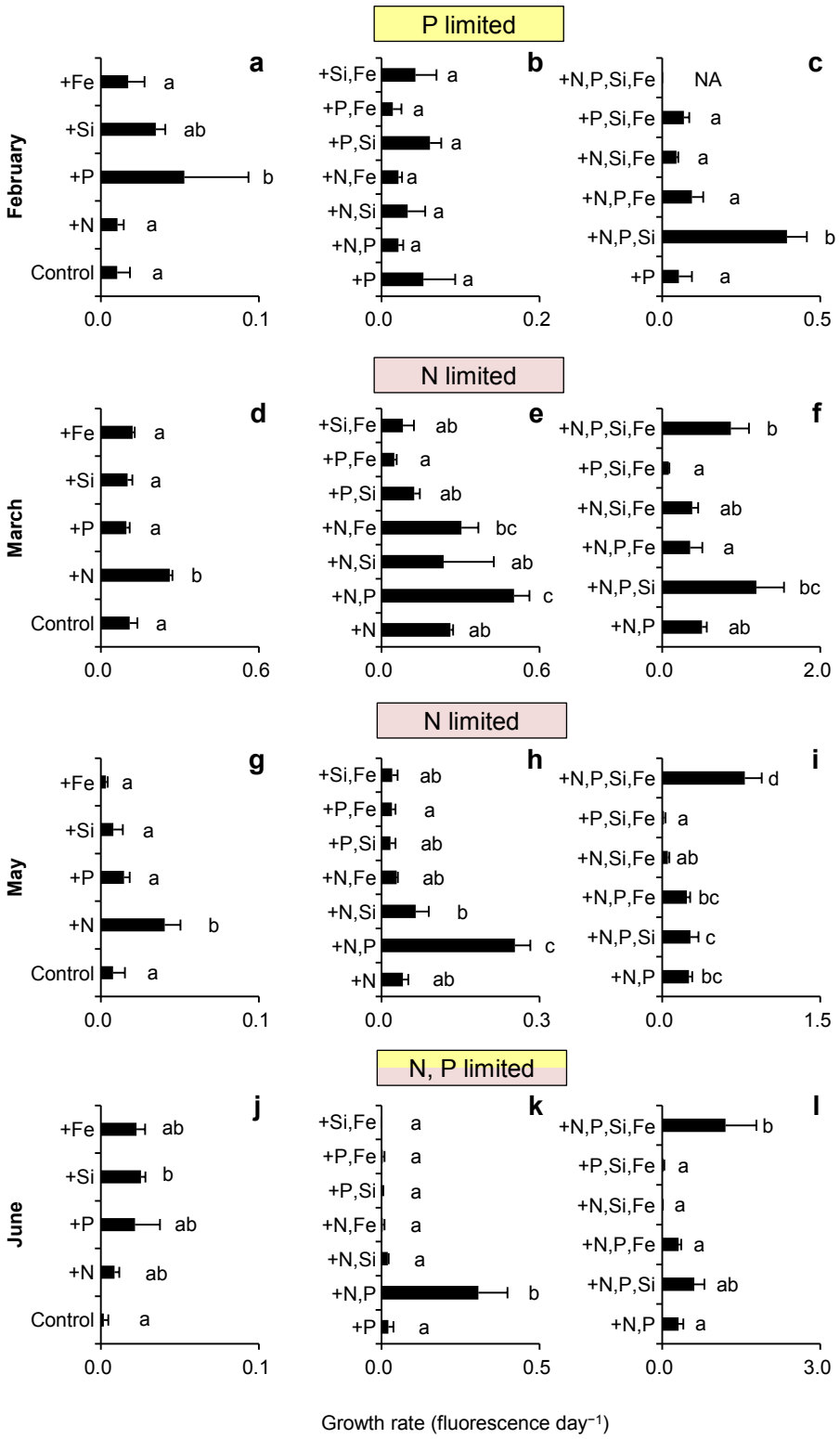
P limited
N limited
N limited
N, P limited
February
March
May
June
a
b
c
d
e
f
g
h
i
j
k
l
+Fe
+Si
+P
+N
Control
+Si,Fe
+P,Fe
+P,Si
+N,Fe
+N,Si
+N,P
+N,P,Si,Fe
+P,Si,Fe
+N,Si,Fe
+N,P,Fe
+N,P,Si
NA
0.0
0.1
0.2
0.5
0.6
2.0
1.5
0.3
3.0
Growth rate (fluorescence day⁻¹)

FIG. 7

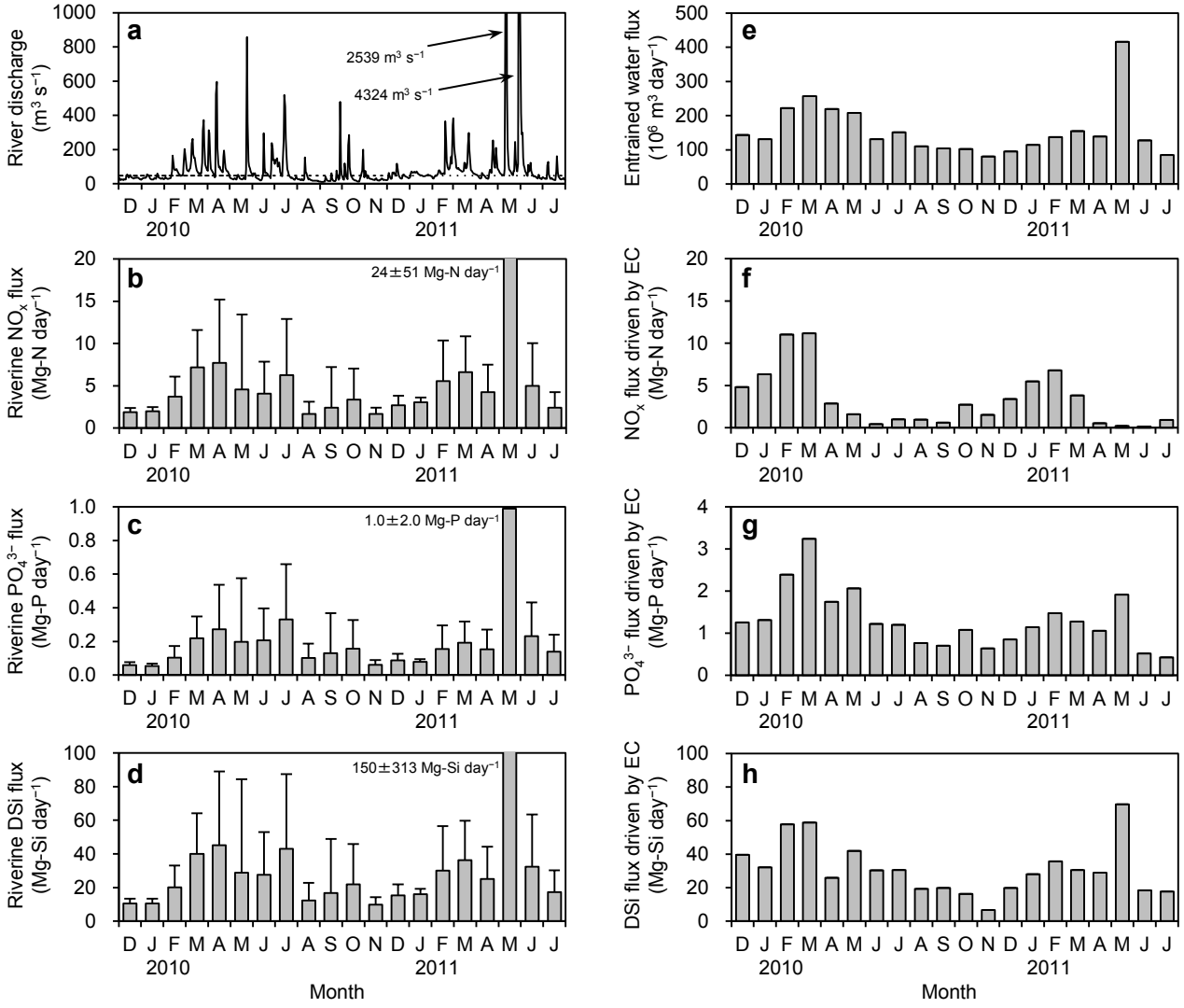
a
River discharge (m³ s⁻¹)
2539 m³ s⁻¹
4324 m³ s⁻¹
b
Riverine NOx flux (Mg-N day⁻¹)
24±51 Mg-N day⁻¹
c
Riverine PO4³⁻ flux (Mg-P day⁻¹)
1.0±2.0 Mg-P day⁻¹
d
Riverine DSi flux (Mg-Si day⁻¹)
150±313 Mg-Si day⁻¹
e
Entrained water flux (10⁶ m³ day⁻¹)
f
NOx flux driven by EC (Mg-N day⁻¹)
g
PO4³⁻ flux driven by EC (Mg-P day⁻¹)
h
DSi flux driven by EC (Mg-Si day⁻¹)
D J F M A M J J A S O N D J F M A M J J
2010
2011
Month

FIG. 8

Table S1. Results of a generalized linear model to estimate extinction coefficients (k) from turbidity.

Coefficients	Estimate	Standard error	p
Intercept	0.162	0.009	<0.001
Turbidity	0.108	0.007	<0.001

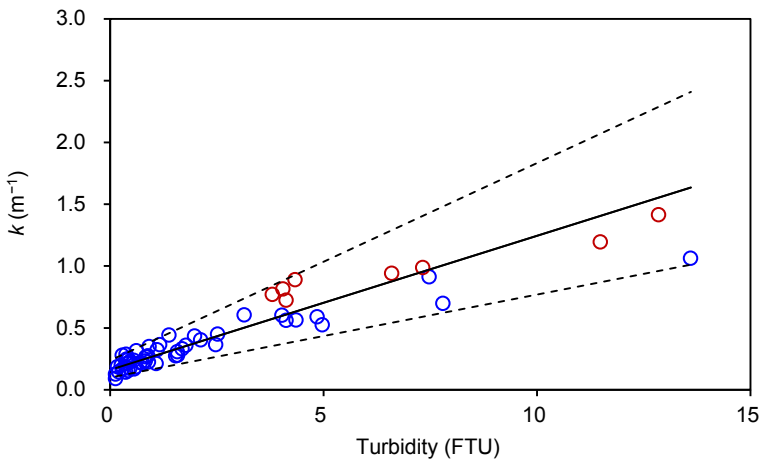

Fig. S1. Relationship between turbidity (FTU) and extinction coefficients (k, m^{-1}) in Tango Bay coastal zone. Red and blue circles indicate surface and bottom waters, respectively. A solid line represents the fitting model of a generalized linear model with identity link and gamma distribution. Dashed lines indicate the 95% prediction interval

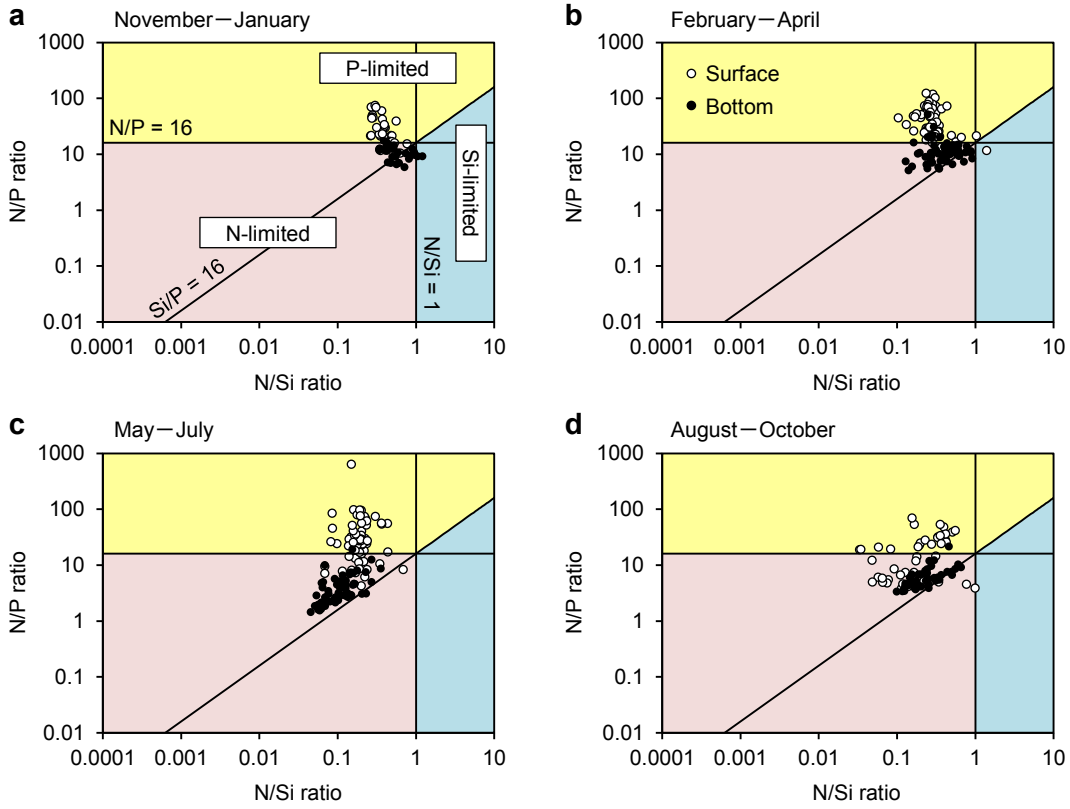

Fig. S2. N:P:Si molar ratios (log N/Si ratio vs. log N/P ratio) in the coastal waters of Tango Bay (**a**) from November to January, (**b**) from February to April, (**c**) from May to July, and (**d**) from August to October in 2010 and 2011. N, P and Si indicate DIN (NO_x + NH_4^+), PO_4^{3-} and DSi, respectively. NH_4^+ concentration data were obtained at stations T1 and T2 from July 2007 to March 2008 (monthly surveys; Watanabe et al., 2014). We used the mean NH_4^+ concentration for each period and layer. The three areas delimited by the Redfield ratio (N:P:Si = 16:1:16) are characterized by different potentially limiting nutrients. Open and closed circles indicate nutrient ratios in the surface and bottom water, respectively